CHROMATOGRAPHIC STUDY OF DIFFUSION IN MOLECULAR-SIEVING CARBON*

KUNITARO KAWAZOE, MOTOYUKI SUZUKI
AND KAZUYUKI CHIHARA
Institute of Industrial Science, University of Tokyo, Tokyo

Chromatographic measurements were made for nitrogen adsorption on molecular-sieving carbons at 60, 100 and 150°C for several different nitrogen surface coverages.

Apparent adsorption equilibrium constants were determined from the retention times of the peaks for different concentrations, and the adsorption equilibrium isotherms were then determined. The peak width gave the intra-microparticle diffusivity where the effects of all the other possible transport processes were taken into account.

The strong dependence of the diffusivity on the amount adsorbed was explained in terms of chemical potential gradient as a driving force of the diffusion.

Introduction

Molecular-sieving activated carbon (MSC) has several unique features. Micropores form slits of about 5 Å opening, whereas conventional molecular-sieving materials such as zeolite, faujasite and mordenite have network structures or straight pores. The well-defined structure of graphite carbon which composes a slit wall is of interest from the standpoint of equilibrium and rate studies of adsorption in micropores of activated carbons.

Kawazoe *et al.*[3-5] reported an extensive study of adsorption equilibrium characteristics of molecular-sieving carbon. However, there has been no work done on diffusion in micropores of molecular-sieving carbon.

This paper is concerned with the rate of nitrogen adsorption in molecular-sieving carbon. The effective diffusivities of nitrogen in micropores were determined by means of a chromatographic technique. Since the adsorption isotherms are non-linear, a small perturbation pulse of nitrogen was introduced to the steady flow of a given nitrogen concentration in a packed bed of molecular-sieving carbon particles and the response was then analysed by using the theory of linear non-equilibrium chromatography. In this way the effective diffusivities of nitrogen in micropores were obtained for several surface coverages of nitrogen at 60, 100 and 150°C.

Theory of Chromatography

Suppose the adsorption isotherm is given as

$$Q=Q(C) \tag{1}$$

When a small change of concentration $c(t)$ is superposed on the steady-state concentration C_0, the corresponding change of amount adsorbed $q(t)$ can be expressed as

$$q=K^*\cdot c \tag{2}$$

where K^* is an apparent equilibrium constant

$$K^*=(dQ/dC)_{C=C_0} \tag{3}$$

Figure 1 illustrates this concept.

The differential equations which describe $c(t)$ in a packed bed of spherical particles with bidispersed pore structure, such as the MSC employed here, are as follows:

material balance in the bed

$$E_z\cdot\frac{\partial^2 c}{\partial z^2}-u\frac{\partial c}{\partial z}-\frac{3(1-\varepsilon)}{\varepsilon R}N_o=\frac{\partial c}{\partial t} \tag{4}$$

material balance at the external surface of particles

$$N_o=k_f(c-c'|_{r_a=R})=D_a\frac{\partial c'}{\partial r_a}\bigg|_{r_a=R} \tag{5}$$

material balance in a particle

$$\frac{D_a}{\varepsilon_a}\left(\frac{\partial^2 c'}{\partial r_a^2}+\frac{2}{r_a}\frac{\partial c'}{\partial r_a}\right)-\frac{3(1-\varepsilon_a)}{\varepsilon_a\cdot a}\cdot\frac{\rho_p}{1-\varepsilon_a}N_i=\frac{\partial c'}{\partial t} \tag{6}$$

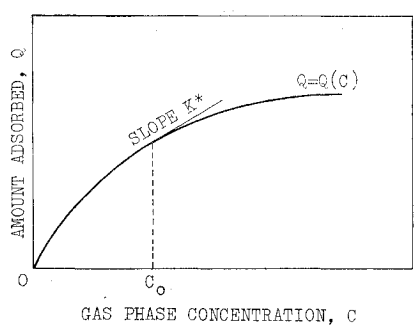

Fig. 1 Adsorption isotherm and apparent equilibrium constant

* Received on October 13, 1973
〒106 東京都港区六本木7-22-1
東京大学生産技術研究所　茅原一之

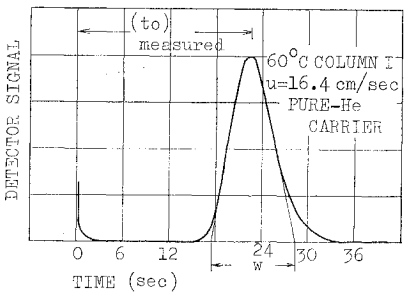

Fig. 2 Typical chromatogram

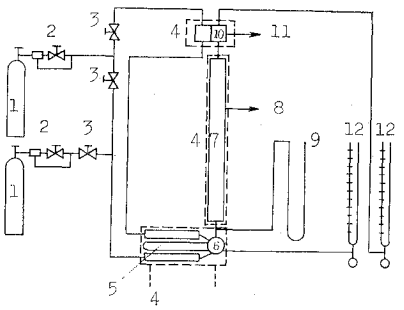

1. cylinder
2. pressure regulator
3. needle valve
4. constant temperature bath
5. pulse injection
6. 6-way valve
7. adsorbent bed
8. temperature measurement
9. pressure gauge
10. T. C. cell
11. recorder
12. soap flow meter

Fig. 3 Schematic diagram of experimental apparatus

material balance at the surface of micro-particles

$$N_i=D\frac{\partial q}{\partial r_i}\bigg|_{r_i=a} \tag{7}$$

adsorption which is in equilibrium at the surface of micro-particles

$$q=K^*c' \tag{8}$$

material balance in the interior of a micro-particle

$$D\left(\frac{\partial^2 q}{\partial r_i^2}+\frac{2}{r_i}\frac{\partial q}{\partial r_i}\right)=\frac{\partial q}{\partial t} \tag{9}$$

The above equations are based on the model in which small micro-particles of radius a are pelletized to form a macro-particle of radius R. Then inter-micro-particle spaces remain as macropores and adsorption takes place at the surface of micro-particles, which is followed by sorption into micro-particles.

The Eqs. (4)–(9) have been solved in Laplace domain to give the moments of the impulse response[7]. The results are as follows:

$$\mu_1\equiv\int_0^\infty C_e(t)\cdot t dt$$
$$=\frac{z}{u}\left\{1+\frac{(1-\varepsilon)\varepsilon_a}{\varepsilon}\left(1+\frac{\rho_p}{\varepsilon_a}K^*\right)\right\} \tag{10}$$

$$\mu_2'\equiv\int_0^\infty C_e(t)\cdot(t-\mu_1)^2 dt$$
$$=\frac{2z}{u}\{\delta_d+\delta_f+\delta_a+\delta_i\} \tag{11}$$

$$\delta_d=\frac{E_z}{u^2}\left\{1+\frac{(1-\varepsilon)\varepsilon_a}{\varepsilon}\left(1+\frac{\rho_p}{\varepsilon_a}K^*\right)\right\}^2 \tag{11a}$$

Table 1 Properties of molecular-sieving carbon[4]

Particle density, ρ_p [g/cm³]	0.90
True density [g/cm³]	1.8
Macropore volume [cm³/g·carbon]	0.38
Micropore volume [cm³/g·carbon]	0.18
Total pore volume [cm³/g·carbon]	0.56
Porosity of macropore, ε_a [−]	0.342
Macropore radius [μ]	2.0
Micropore opening [Å]	5

$$\delta_f=\frac{1-\varepsilon}{\varepsilon}\cdot\frac{R\varepsilon_a^2}{3k_f}\left(1+\frac{\rho_p}{\varepsilon_a}K^*\right)^2 \tag{11b}$$

$$\delta_a=\frac{1-\varepsilon}{\varepsilon}\cdot\frac{R^2\varepsilon_a^2}{15D_a}\left(1+\frac{\rho_p}{\varepsilon_a}K^*\right)^2 \tag{11c}$$

$$\delta_i=\frac{1-\varepsilon}{\varepsilon}\cdot\frac{a^2}{15D}\cdot\rho_p K^* \tag{11d}$$

When the output signal $c_e(t)$ can be approximated by the normal distribution curve, the first absolute moment and the second central moment are readily related to the position and the width of the peak, respectively. **Figure 2** illustrates this procedure. The position of the peak t_0 is taken as μ_1 and the tangents at the inflexion points are used to determine the width w of the peak. Then the second central moment μ_2' is calculated from w by the equation

$$\mu_2'=\frac{w^2}{16} \tag{12}$$

Experimental

Apparatus

The schematic diagram of the apparatus is shown in **Fig. 3**. The apparatus was similar to a conventional gas chromatograph. A pulse of the gas mixture, the nitrogen concentration of which differs by less than 2.0 vol% from that of the carrier gas mixture, was introduced into the carrier gas stream by a 6-way valve. Pulse volume was fixed to be 2.5 cc. The stream then flowed through the bed of adsorbent particles. The effluent was passed through the sample side of the thermal conductivity cell. The equipment was designed to minimize the volume in the lines between the detector and the bed and between the valve and the bed. Adsorbent particles were packed in a glass tube, which was kept at a constant temperature by a ribbon-heater equipped with a regulator.

Gases

The purity of the helium was specified to be 99.995%, while the nitrogen was technical grade (99.9% purity). Helium, nitrogen and helium-nitrogen mixtures were used as carrier gases. Mixtures were prepared in cylinders by introducing calculated pressures of nitrogen and helium. Resultant concentration was determined by comparing the peak area of the mixture pulse in a pure helium carrier with that of a pure nitrogen pulse. The proportionality between the nitrogen concentrations and the peak areas at the

Table 2 Experimental condition

	Column I												Column II	
Range of sieve openings [mm]	1.190–1.680												0.540–0.840	
Average particle radius [mm]	0.707												0.337	
Column diameter [mm]	9.8												5.3	
Cross sectional area of the column [cm²]	0.754												0.222	
Length of the packed bed [cm]	44.3												51.5	
Mass of adsorbent [g]	16.8												5.26	
Void fraction, ε [—]	0.442												0.489	
Column temp. [°C]	60				100				150				60	150
Conc. of carrier gas [N_2%]	0	41.2	63.3	100	0	41.2	63.3	100	0	41.2	63.3	100	0	0
Interstitial velocity, u [cm/sec]	1.57	5.79	4.25	2.42	2.22	6.26	3.80	2.56	1.19	4.93	4.19	2.15	4.56	5.56
	35.2	30.5	21.9	13.7	33.9	34.6	25.4	16.8	77.4	34.2	23.7	19.5	79.8	115

outlet of the column was found to be excellent. The sample gas mixture was made by mixing the carrier gas and the nitrogen (or helium, when pure nitrogen was used as a carrier) in the sample gas line. The mixing ratio of the pulse gas mixture was fixed to be 2.00 vol% of the carrier gas during the whole experiment.

Adsorbent particles

The molecular-sieving carbon was provided by Takeda Chemical Co. (MSC 5A–HGS 638). The pellets have a bidispersed pore structure. The micropore forms a slit of 5 Å opening, which has been proved by the molecular-probe technique[2]. The properties of the MSC 5 A are shown in **Table 1**. The pore-volume distribution measured by mercury porosimeter for the range 0.03–50 μ is given in ref. 3). The original pellets were crushed and screened to yield the desired sizes of small particles. Before the runs the bed of adsorbent particles was degassed by passing pure helium through the bed for 2–3 hr at 250°C.

Bed characteristics

The properties of the packed beds are shown in **Table 2**. The average particle diameter assigned for each size was taken as the arithmetic average of the maximum and minimum sieve openings. The porosities in the beds were estimated from bed volume, mass and particle apparent density.

Experimental program

First, runs were made with pure helium carrier at 60, 100 and 150°C and varying the flow rates to establish the influence of axial dispersion in Column I. Next, runs were made with Column II in the same way to check the contributions of macropore resistance. These data, combined with the first data, gave sets of D and K^* values for a nitrogen pressure near zero. Finally, nitrogen pulses diluted with the carrier were introduced into a stream of helium-nitrogen mixture. By using different compositions of the helium-nitrogen mixture, it was possible to obtain D and K^* over a range of nitrogen pressure from 0–760 mmHg. These runs were made at 60, 100 and 150°C in Column I. The volumetric flow rate of carrier gas was varied from about 0.58 to 9.4 cm³/sec (room temperature and 1 atm). This corresponded to a range of interstitial velocity from about 2.2 to 34 cm/sec for runs at 100°C.

Typical chromatogram is shown in Fig. 2.

Table 3 Apparent equilibrium constant, K^* [cc/g·carbon]

Column temp. [°C]	Concentration of nitrogen in carrier gas [N_2, vol%]			
	0	41.2	63.3	100
60	6.14	3.10	2.17	0.456
100	3.75	2.27	1.49	0.491
150	2.13	1.43	1.05	0.454

Results and Discussion

Apparent adsorption equilibrium constant

Dead volume correction was first made for t_0 obtained from a chromatogram. Volume of the pipes between the six-way valve and the inlet of the bed and between the outlet of the bed and the detector was about 2.4 cc. Then t_0 was calculated as

$$t_0=(t_0)_{\text{measured}}-\frac{2.4}{v} \tag{13}$$

From Eq. (10), it follows that

$$\phi=\frac{\varepsilon\cdot\Delta t_0}{(1-\varepsilon)}=\frac{z}{u}\rho_p K^* \tag{14}$$

$$\Delta t_0=t_0-(t_0)_{\text{inert}} \tag{15}$$

The retention time for an inert pulse ($K^*=0$) is given from Eq. (10).

$$(t_0)_{\text{inert}}=\frac{z}{u}\cdot\left(1+\frac{1-\varepsilon}{\varepsilon}\varepsilon_a\right) \tag{16}$$

According to Eq. (14), plots of the retention time function ϕ versus z/u should be a straight line of the slope $\rho_p K^*$. It is apparent in **Fig. 4** that a well-defined linear relation holds for each nitrogen concentration of the carrier. Apparent adsorption equilibrium constant K^* calculated from the slope of the ϕ-plot for each condition is listed in **Table 3**. Ex-

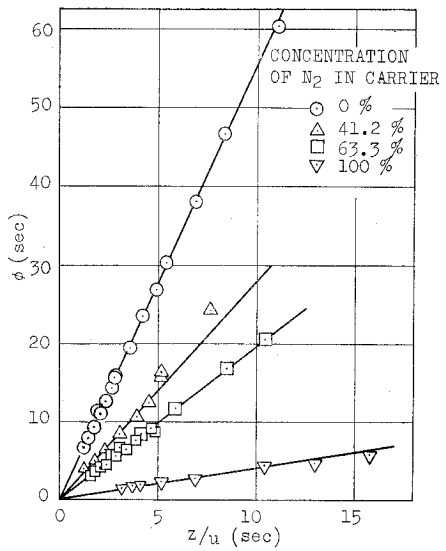

Fig. 4 First moment plots for different concentrations at 60°C (Column I)

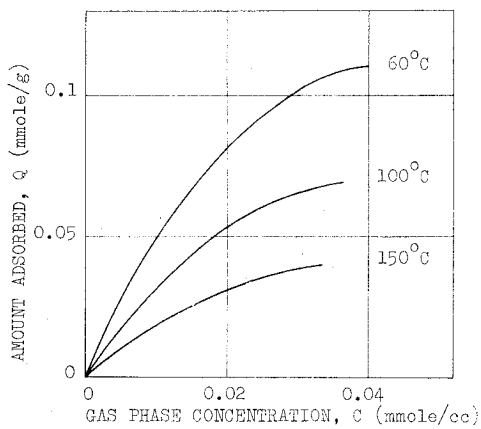

Fig. 5 Adsorption isotherms for different temperatures

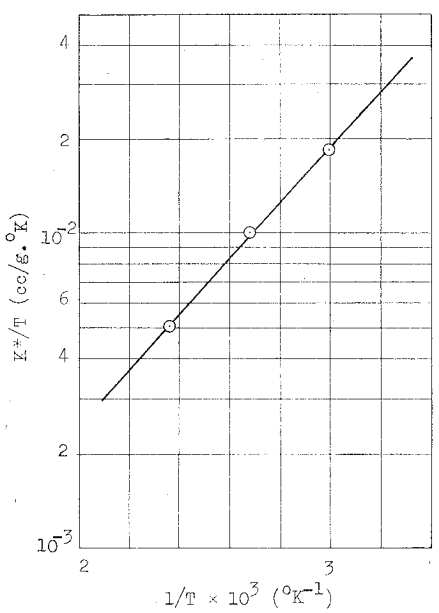

Fig. 6 Apparent equilibrium constant at $C_0=0$

pectedly, K^* decreases when the concentration of nitrogen (C_0) increases in a carrier gas stream.

For each temperature, the isotherm Q vs. C can be obtained by graphical integrations of the curve, K^* vs. C_0, obtained from the experiment. This is shown in **Fig. 5**. Detailed discussion based upon the isotherm thus determined is not possible, since the graphical integration from only four points leaves a question of accuracy, but the shape of the isotherm for each temperature seems quite reasonable and the isosteric heat of adsorption can be determined by the equation.

$$q_{iso}=R_g T^2\left(\frac{\partial \ln p}{\partial T}\right)_Q$$

$$=R_g\left(\frac{\Delta \ln(K^*/T)}{\Delta(1/T)}\right)_Q \qquad (17)$$

By using the values of K^* at $C_0=0$ ($Q=0$), q_{iso} is calculated to be 4.0 Kcal/mole, about the right order of magnitude as the physical adsorption of nitrogen. Plots of $\ln(K^*/T)_{C_0=0}$ versus $1/T$ according to Eq. (17) are shown in **Fig. 6**.

Transport properties in the bed

The second moment equation (Eq. (11)) includes the effects of axial dispersion and external mass transfer as the bed properties. External mass transfer is expected to be less significant compared with axial dispersion or intraparticle properties[9]. Also, the established relation proposed by Carberry[1] gives a reasonably accurate estimate of the external mass transfer coefficient:

$$\left(\frac{k_f d_p}{D_v}\right)=1.15\left(\frac{\nu}{D_v}\right)^{1/3}\left(\frac{d_p u}{\nu}\right)^{1/2} \qquad (18)$$

Then δ_f in Eq. (11) was first calculated from Eq. (18) and the following function, Δ, was used to clarify the effect of axial dispersion

$$\Delta=\frac{\mu_2'}{2z/u}-\delta_f \qquad (19)$$

$$=\delta_d+\delta_a+\delta_i \qquad (20)$$

where δ_d, δ_a and δ_i are given in Eqs. (11a)–(11d) and only δ_d is dependent on velocity. Usually axial dispersion coefficient E_z is expressed as the sum of the contribution of molecular diffusion and that of fluid dispersion in the bed

$$E_z=\frac{D_v}{\tau_{ext}}+\frac{d_p u}{Pe} \qquad (21)$$

Pe is a constant defined as $d_p u/E_{z,f}$ where $E_{z,f}$ is a dispersion coefficient due to fluid mixing.

At higher velocities, the second term in Eq. (21) is expected to become dominant, and Δ is plotted against $1/u$ to estimate $(\delta_a+\delta_i)$ from the intercept at $1/u=0$. **Figure 7** shows typical examples of the above plots for Column I for different concentrations at 60°C.

From high-velocity data $Pe=1.2$ and 0.51 were

Table 4 Δ_0 and D/a^2 for each condition

Temp. [°C]	Concentration of nitrogen in carrier gas [N_2, vol%] 0		41.2		63.3		100	
	Δ_0 [sec]	D/a^2 [sec^{-1}]	Δ_0	D/a^2	Δ_0	D/a^2	Δ_0	D/a^2
60	0.624	1.01	0.169	1.91	0.08_4	2.19	0.006_8	10.4
100	0.224	1.65	0.095_9	2.33	0.047_2	3.15	0.008_7	5.98
150	0.064_7	3.33	0.035_5	3.97	0.019_8	5.46	0.005_2	10.9

determined for Column I (d_p=1.41 mm) and II (d_p=0.67 mm), respectively. These values were in good agreement with the previous data for packed beds of small particles[10] and were used for correlating the other runs together with external tortuosity factor τ_{ext}=1.4 by means of Eq. (21). The solid lines in Fig. 7 show δ_d thus calculated for Column I at 60°C.

Intraparticle properties

The intercepts of the plot Δ vs. $1/u$ at $1/u=0$, Δ_0, give $(\delta_a+\delta_i)$ as is clear from Eq. (20).

For the diffusivity in macropores, D_a, parallel pore model gives

$$D_a=\frac{\varepsilon_a}{\tau_p}D_v \tag{22}$$

where τ_p is the tortuosity factor of macropores, which is of the order of 3 to 4 for activated carbons[6]. The effect of macropore diffusivity can be checked by employing different sizes of carbon particles. That is, δ_a has strong dependence on particle size, R, while δ_i is independent of R. Then the plots of $\{\varepsilon/(1-\varepsilon)\}(\delta_a+\delta_i)/(\varepsilon_a+\rho_pK^*)^2$ versus R^2 should give D_a and $\{\varepsilon/(1-\varepsilon)\}\delta_i/(\varepsilon_a+\rho_pK^*)^2$ from the slope of the plots and the intercepts respectively. This was done in **Fig. 8** for the two sets of conditions (60°C and 150°C, pure helium runs), where $(\delta_a+\delta_i)$ from Column II was also included. Solid lines in the figure correspond to the values of D_a estimated from Eq. (22) by taking τ_p=3.2. The plot suggests that τ_p=3.2 is reasonable, and this figure was used for the correction of δ_a for the other conditions.

Diffusivity in micropores

After correction for macropore diffusivity, D/a^2 for each condition is obtained from $\{\varepsilon/(1-\varepsilon)\}\delta_i/(\rho_pK^*+\varepsilon_a)^2$ by the equation

$$\frac{D}{a^2}=\frac{\rho_pK^*}{15(\rho_pK^*+\varepsilon_a)^2}\Big/\left\{\frac{\varepsilon}{1-\varepsilon}\delta_i\Big/(\rho_pK^*+\varepsilon_a)^2\right\} \tag{23}$$

The final results of D/a^2 together with $\Delta_0=(\delta_a+\delta_i)$ for all the conditions are listed in **Table 4.**

The diffusivity D is defined on the basis of adsorbed concentration gradient driving force. If the diffusion in micropore is governed by diffusion of Knudsen type, then $D\cdot(\rho_pK^*)/(1-\varepsilon_a)$ should be of the same order of magnitude as the value given by the equation.

$$D_K=\frac{4}{3}\bar{r}\left(\frac{2R_gT}{\pi M}\right)^{1/2} \tag{24}$$

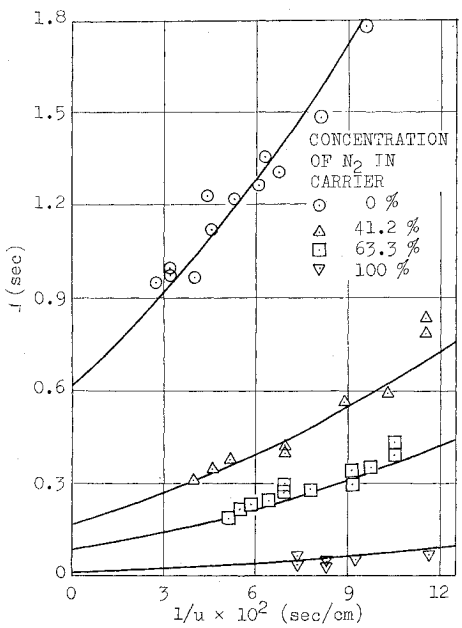

Solid lines are based on Eq. (21) with Pe=1.2 and τ_{ext}=1.4

Fig. 7 Second moment plots for different concentrations at 60°C (Column I)

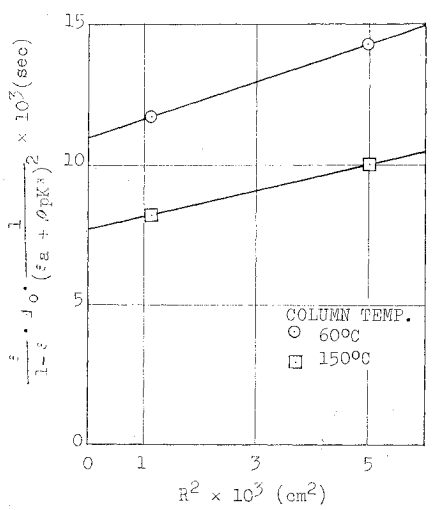

Fig. 8 Plots of $\{\varepsilon/(1-\varepsilon)\,(\varepsilon_a+\rho_pK^*)^2\}\cdot\Delta_0$ versus R^2

The radius of a micro-particle is expected to be about 6 μ from the size of macropore (2 μ)[3]. Numerical comparison at 100°C by using a=6 μ shows that $D\cdot(\rho_pK^*)/(1-\varepsilon_a)=5.5\times10^{-6}$ cm²/sec for C_0=0 while D_K is 8.9×10^{-4} cm²/sec from Eq. (24). Therefore the diffusion in micropores is far more restricted than Knudsen-type diffusion. Then it might be plausible to consider it as diffusion of activated type, which

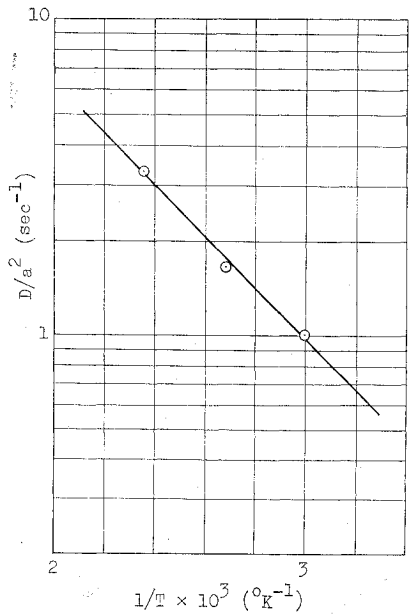

Fig. 9 Dependence of diffusivity at $C_0=0$ on temp.

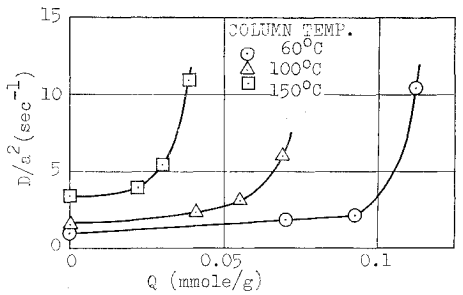

Fig. 10 Dependence of diffusivity on amount adsorbed at 60, 100 and 150°C

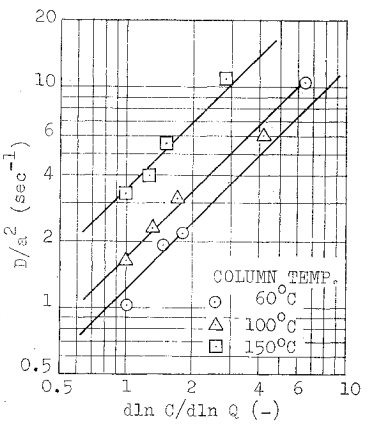

Fig. 11 Plots of D/a^2 versus $d\ln C/d\ln Q$

occurs when the size of the diffusing species is close to the pore opening. This is common in other molecular-sieving materials such as zeolites. The values of D/a^2 at $C_0=0$ for different temperatures are plotted in Arrhenius' way in **Fig. 9**. The resulting activation energy was 3.7 kcal/mole, which is a little less than the isosteric heat of adsorption.

Figure 10 illustrates the dependence of D/a^2 on the amount adsorbed, Q, which is estimated from the isotherm shown in Fig. 5. Strong dependence of

Table 5 Mobility coefficient of nitrogen on molecular-sieving carbon

Temp. [°C]	RTB/a^2 [1/sec]	B [mole·cm²/kcal·sec]
60	1.2	6.5×10^{-16}
100	1.7	8.3×10^{-16}
150	3.5	1.5×10^{-15}

D/a^2 on Q was also shown in the case of adsorption in zeolites[8]. Since the driving force for the diffusion flux in micropores is essentially the gradient of chemical potential per molecule, the flux is expressed as

$$N=-B\cdot Q\cdot\frac{d\mu}{dx} \tag{25}$$

Where B is the intrinsic mobility of diffusing species. The chemical potential is replaced by the activity a by the equation

$$d\mu=RTd\ln a \tag{26}$$

and then Eq. (25) becomes

$$N=-RT\cdot B\frac{d\ln a}{d\ln Q}\frac{dQ}{dx} \tag{27}$$

In the present case, since $Q=Q(C_0)+q(x,t)$, the flux equation in the micropore becomes

$$N=-D\cdot\frac{dq}{dx} \tag{28}$$

$$D=B\cdot RT\cdot\frac{d\ln C}{d\ln Q} \tag{29}$$

where activity a is assumed to be equal to the gas-phase concentration C which is in equilibrium with the amount adsorbed Q. Since $d\ln C/d\ln Q$ can be determined from the isotherm shown in Fig. 5, D/a^2 is plotted against corresponding $d\ln C/d\ln Q$ for each condition in **Fig. 11**. The plots show that there exist linear relations between D/a^2 and $d\ln C/d\ln Q$ for each temperature. This suggests that the diffusion in micropores in MSC is controlled by the chemical potential driving force. The slope of the straight line gives RTB/a^2. The intrinsic mobility, B, determined by assuming $a=6\ \mu$, is included in **Table 5**.

Conclusion

Chromatographic measurements were made for nitrogen adsorption on molecular-sieving carbons at 60, 100 and 150°C and for several nitrogen surface concentrations.

Adsorption equilibrium isotherms were determined from the retention time of the peak, and the peak width gave the intra-micropore diffusivity where the effects of all the other possible transport processes were taken into account.

The dependence of diffusivity on the amount adsorbed was explained in terms of diffusion by chemical potential driving force.

It was shown through this study that chromatographic technique is especially helpful for the determination of micropore diffusivity when the time constant of diffusion (δ_i) is of the order of or less than a few seconds, which would often be the case in reacting systems. In the case where much larger time constant is involved, conventional electrobalance technique can provide reasonable data on adsorption rates.

Nomenclature

a	=	radius of micro-particle	[cm]
B	=	intrinsic mobility	[mole/cm·atm·sec]
C	=	concentration in the fluid phase	[mole/cc]
C_0	=	concentration in the carrier gas	[mole/cc]
c	=	concentration change in the fluid phase	[mole/cc]
c'	=	concentration change in the particle	[mole/cc]
D	=	diffusivity in micropores based on amount adsorbed gradient driving force	[cm²/sec]
D_a	=	diffusivity in macropores	[cm²/sec]
D_v	=	molecular diffusivity	[cm²/sec]
D_K	=	Knudsen diffusivity	[cm²/sec]
d_p	=	particle diameter	[cm]
E_z	=	axial dispersion coefficient based on void spaces in the bed	[cm²/sec]
$E_{z,f}$	=	dispersion coefficient due to fluid mixing	[cm²/sec]
K^*	=	apparent adsorption equilibrium constant	[cc/g]
k_f	=	external mass transfer coefficient	[cm/sec]
M	=	molecular weight	[g/mole]
N	=	mass flux	[mole·cm/g·sec]
N_i	=	flux at the surface of micro-particle	[mole·cm/g·sec]
N_o	=	flux at the external surface of particles	[mole/cm²·sec]
p	=	pressure of adsorbate in the fluid phase	[mmHg]
Pe	=	Peclet number, $d_p u/E_{z,f}$	[—]
Q	=	amount adsorbed per unit mass of adsorbent	[mole/g]
q	=	change of amount adsorbed	[mole/g]
q_{iso}	=	isosteric heat of adsorption	[kcal/mole]
R	=	radius of particle	[cm]
R_g	=	gas constant	[—]
r_a	=	radial position in a particle	[cm]
$\bar{r}$	=	average pore radius	[cm]
r_i	=	radial position in a micro-particle	[cm]
T	=	absolute temperature	[°K]
t	=	time	[sec]
t_0	=	position of the chromatographic peak in time scale	[sec]
u	=	interstitial velocity of fluid	[cm/sec]
v	=	volumetric flow rate	[cc/sec]
w	=	peak width defined in Fig. 2	[sec]
z	=	longitudinal position in the bed	[cm]
α	=	activity of a diffusing species	[—]
Δ	=	defined by Eq. (19)	[—]
$\delta_a, \delta_i, \delta_d, \delta_f$	=	defined by Eqs. (11a)–(11d)	[—]
ε	=	void fraction in the bed	[—]
ε_a	=	macropore fraction in the particle	[—]
μ	=	chemical potential	[atm·cc/mole]
μ_1	=	first absolute moment of the chromatographic peak	[sec]
μ_2'	=	second central moment	[sec²]
ν	=	kinematic viscosity	[cm²/sec]
ρ_p	=	particle density	[g/cc]
τ_{ext}	=	tortuosity factor of interstitial fluid path	[—]
τ_p	=	tortuosity factor of macropores	[—]

Literature Cited

1) Carberry, J. J.: *AIChE J.*, **6**, 460 (1960)
2) Eguchi, Y.: *Kagaku Kojo*, **13**, 49 (1969)
3) Kawazoe, K., V. A. Astakhov and T. Kawai: *Seisankenkyu, Jl., Inst. Ind. Sci., University of Tokyo*, **22**, 491 (1970)
4) Kawazoe, K., V. A. Astakhov, T. Kawai and Y. Eguchi: *Kagaku Kōgaku*, **35**, 1006 (1971)
5) Kawazoe, K., T. Kawai, Y. Eguchi and K. Itoga: Submitted to *J. Chem. Eng. Japan*
6) Kawazoe, K., I. Sugiyama and Y. Fukuda: *Kagaku Kōgaku*, **30**, 1007 (1966)
7) Kawazoe, K., M. Suzuki and K. Chihara: *Seisankenkyu, Jl., Inst. Ind., Sci., University of Tokyo*, **25**, 558 (1973)
8) Ruthven, D. M. and K. F. Loughlin: *Chem. Eng. Sci.*, **26**, 1145 (1971)
9) Schneider, P. and J. M. Smith: *AIChE J.*, **14**, 762 (1968)
10) Suzuki, M. and J. M. Smith: *The Chem. Eng. Jl.*, **3**, 256 (1972)